Article

Numerical Investigation of Heat Transfer Enhancement in a Microchannel with Conical-Shaped Reentrant Cavity

Syarif Syahrul Syazwan Muzhaimey [1], **Nik Nazri Nik Ghazali** [1,*], **Mohd Zamri Zainon** [1], **Irfan Anjum Badruddin** [2,*], **Mohamed Hussien** [3,4], **Sarfaraz Kamangar** [2] **and N. Ameer Ahammad** [5]

1 Department of Mechanical Engineering, Faculty of Engineering, University of Malaya, Kuala Lumpur 50603, Malaysia
2 Mechanical Engineering Department, College of Engineering, King Khalid University, Abha 61421, Saudi Arabia
3 Department of Chemistry, Faculty of Science, King Khalid University, P.O. Box 9004, Abha 61413, Saudi Arabia
4 Pesticide Formulation Department, Central Agricultural Pesticide Laboratory, Agricultural Research Center, Dokki, Giza 12618, Egypt
5 Department of Mathematics, Faculty of Science, University of Tabuk, Tabuk 71491, Saudi Arabia
* Correspondence: nik_nazri@um.edu.my (N.N.N.G.); magami.irfan@gmail.com (I.A.B.)

Abstract: The current study is focused on improving the thermal performance of the microchannel heat sink (MCHS) using the passive reentrant cavity approach. The MCHS physical model's single channel was used in a three-dimensional numerical simulation. The basic geometrical layout of the MCHS's computational domain was drawn from previously published research and verified using numerical and analytical correlations that were already in existence. The innovative conical-shaped microchannel heat sink's (CMCHS) properties for heat transmission and fluid flow were examined numerically under steady-state conditions with laminar flow and a constant heat flux. At various flow velocities and configurations, the impacts of the geometrical parameters on pressure drops and heat transfer were examined. The outcome demonstrates a tremendously positive thermal performance with a significantly greater pressure drop than the traditional straight channel. In the microchannels with the conical-shaped reentrant cavities and minimal pressure loss, convection heat transfer is significantly improved. The findings of the present investigation demonstrate that the conical-shaped MCHS is practical and has a good chance of being used in real-world settings.

Keywords: heat flux; convection; microchannel; laminar

MSC: 76-10

1. Introduction

The need for high heat dissipation in microelectronic systems and nanotechnologies has accelerated, making the cooling mechanism one of the primary issues in order to stop hot zones from forming. To solve this problem and provide efficient heat removal, many researchers have developed a variety of approaches, including fuel cells, microreactors, and microheat sinks. Numerous researchers have looked at the use of microchannels in devices with high heat dissipation after being inspired by the pioneering work of Tuckerman and Pease [1]. The microchannel heat sink (MCHS), which can remove heat at a rate of up to 790 W/cm^2 [2], is seen to be the most promising method for addressing the cooling issues faced by the electromechanical industry. The microchannel size of the channel in the traditional straight, rectangular MCHS only permits fluid flow to be in the laminar flow regime, preventing the formation of turbulent flow. Researchers have examined the efficacy of several techniques to raise the MCHS heat removal rate. In an experiment, Peng and Peterson [3] discovered that the modifications to the geometric configuration significantly improved the single-phase MCHS's convectional heat transfer and flow characteristics.

Adams et al. [4] said that a substantial quantity of heat could be transmitted out in microchannels with built-in chip substrates with a small temperature difference between

the fluid and solid contact. Researchers have tried to change the cross-section region's shape in the microchannels in order to improve heat transmission performance. In order to improve the transfer of heat in single-phase flow, Tao et al. [5] proposed three strategies: increasing the velocity gradient near the heated sidewalls, reducing the thickness of the thermal boundary layer, and elevating disruption in the fluid flow to improve the transfer of heat. The importance of active and passive heat transfer augmentation techniques in mini- and microchannels have been examined by Steinke & Kandlikar [6]. In-depth administration and discussion have been conducted regarding the potential for applying the comprehensive enhancement methods with novel applications in MCHS, including the possibility of flow disruption, channel curvatures, reentrant obstructions, out-of-plane mixing, secondary flows, fluid additives, surface treatment, and surface roughness. The relationship between various cross-sectional area shapes in microchannels and their impacts on increasing heat transfer has been researched by Gunnasegaran et al. [7]. The microchannel with the rectangular cross-section has the highest heat transfer enhancement, while the MCHS with the triangle shape has the lowest performance. Three shapes were introduced. Alfaryjat et al. [8] conducted a numerical analysis of the influence of geometrical parameters on the thermal efficiency of microchannels, taking into account the channel forms of a circle, a rhombus, and a hexagon. The findings indicate that whereas microchannels with a hexagonal cross-sections have the highest heat transfer coefficient and pressure drop values, rhombus cross-sections have the highest thermal resistance and friction factor values.

In general, most researchers preferred the passive method since it does not require any external power. The employment of passive augmentation techniques to boost the efficacy of electrical devices with compact designs has been the subject of numerous investigations. In an MCHS with aligned fan-shaped reentrant cavities, Xia et al. [9] investigated the effects of structural parameters on heat transfer and fluid flow. They found that the significant improvement was brought on by the working fluid slipping over at the reentrant cavities, the jet and throttling effects, and the increase in the fluid-to-solid heat transfer contact area provided by the fan-shaped reentrant cavities. In selecting the ideal circumstance for the enhancement of heat transfer, the length ratio, which establishes the number of cavities along the channel and the arcuate area width ratio, were optimized. Chai et al. have performed subsequent studies [10] examining the heat transfer and fluid flow in a microchannel with fan-shaped reentrant cavities as well, but in an offset arrangement, and it was discovered that, despite the variations in the cavity designs, it was comparable to the earlier study. A numerical analysis on microchannels with triangular reentrant cavities was published by Xia et al. in [11]. By adjusting the geometrical parameters of the cavity, they investigate the effects of geometrical structures to discover the perfect thermal design. The maximum heat transfer and the least amount of pressure drop were achieved with the adjusted geometrical parameters and the related Reynolds numbers, with an overall efficiency of greater than 1.4. Chai et al. [12] independently carried out an experiment and numerically examined the heat transfer performance in microchannels with periodic expansion-constriction cross-sections for traditional rectangular straight MCHS, microchannels with fan-shaped reentrant cavities, and microchannels with triangular reentrant cavities. The analysis demonstrates that, in terms of the Nusselt number and the friction factor, the numerical results and the experimental result are in agreement.

Abouali and Baghernezhad [13] previously conducted research on the effectiveness of heat transfer in MCHS with an arc and a rectangular groove. The channel's sides and floor both now have a groove in them. In terms of heat transfer and friction factor, it is discovered that the arc-grooved microchannel outperforms the rectangular-grooved microchannel. The overall finding of this study indicates that the grooved MCHS significantly outperforms the smooth surface microchannels in terms of thermal resistance and Nusselt number. A numerical analysis of the fluid flow and heat transmission mechanisms in trapezoidally grooved microchannels was presented by Kuppusamy et al. [14]. The flow can diverge from the main channel and move toward the grooved area thanks to the manipulation of

the geometric features, which improves flow mixing. They also came to the conclusion that the thermal performance was improved by the increase in pitch size. Ahmed and Ahmed [15] changed the cavity form from a triangular shape to a trapezoidal shape to a rectangular shape in order to investigate the heat transfer and fluid flow in grooved MCHS. They found that "the results revealed that microchannels with trapezoidal groove cavities give the best thermal design with improvements in the Nusselt number and friction factor of 2.35% and 51.59%, respectively".

Triangular chambers and rectangular ribs combined with microchannels have been examined by Li et al. [16]. A significant increase in heat transport, chaotic mixing of cold and hot water, and an amplified mainstream disturbance with a performance assessment factor of 1.619 were the effects of the disruption and regeneration of the thermal boundary layer. Ghani et al. [17] investigated the heat transfer and fluid flow properties of microchannels with sinusoidal cavities and rectangular ribs. They have independently examined the heat transmission capabilities of MCHS with sinusoidal cavities and MCHS with rectangular ribs in order to compare the two. It has been discovered that combining both designs in one MCHS results in significantly better thermal performance. A wavy MCHS design with variations in the wavelength or its amplitude was introduced by Lin et al. [18]. The results demonstrate that a smaller maximum bottom wall temperature difference and lower thermal resistance considerably improved performance. A numerical analysis of the heat transfer and fluid flow properties of a plate-fin MCHS design with trapezoidal chambers and oval fins with and without slots was performed by Alfellag et al. [19] in a more recent work. According to the results, the proposed design's pin aspect ratio is 1.25, the pin distance from cavity center is 0.03 mm, and the slot thickness is 0.008 mm, giving it a higher performance assessment requirement of 1.37.

The present study, which has never been done before, focuses on the heat transfer and fluid flow on MCHS with a conical-shaped reentrant. The performance of such shape is reported for the first time that could lead to significant improvement in the thermal dissipation. The goal of this study is to compare the Nusselt number, performance assessment standards, fluid flow, pressure distribution, and temperature distribution with the traditional straight MCHS. It also aims to optimize the geometrical characteristics of the conical-shaped reentrant cavities.

2. Mathematical Formulation and Numerical Methods

2.1. Physical Model and Assumptions

The geometrical parameter of the computational domain is demonstrated in Figure 1B with the total length (L) of 10 mm, width (W) of 0.3 mm, and the thickness of the silicon substrate (H) of 0.35 mm. The newly proposed microchannel with conical-shaped reentrant cavities consists of two parallel sidewalls with equally sized conical-shaped reentrant cavities which were periodically arranged at an equidistant from each other along the flow direction on each sidewall. The constant cross-section segment of the microchannel has the width (W_c) of 100 μm and the depth (H_c) of 200 μm. As illustrated in Figure 1B, L_{cc} represents the longitudinal length, H_{cc} is the height of a single reentrant cavity, L_p is the distance of peak point from cavity entrance, L_{sc} is the distance between each cavity, and W_{cs} represents the maximum width of the conic-shaped cavity. For the optimum thermal design, three dimensionless parameters were introduced, $\beta = L/n$, $\gamma = W_{cs}/W_c$, and $\delta = L_p/L_{cc}$. A fully developed velocity profile and uniform temperature profile was considered at the inlet. The substrate's sidewalls are symmetric.

The numerical simulation was carried out using water as the working fluid and the following characteristics:

- The flow is 3-dimensional, steady-state, incompressible, laminar.
- Piecewise-linear dynamic viscosity of water temperature.
- Viscous dissipation is considered.
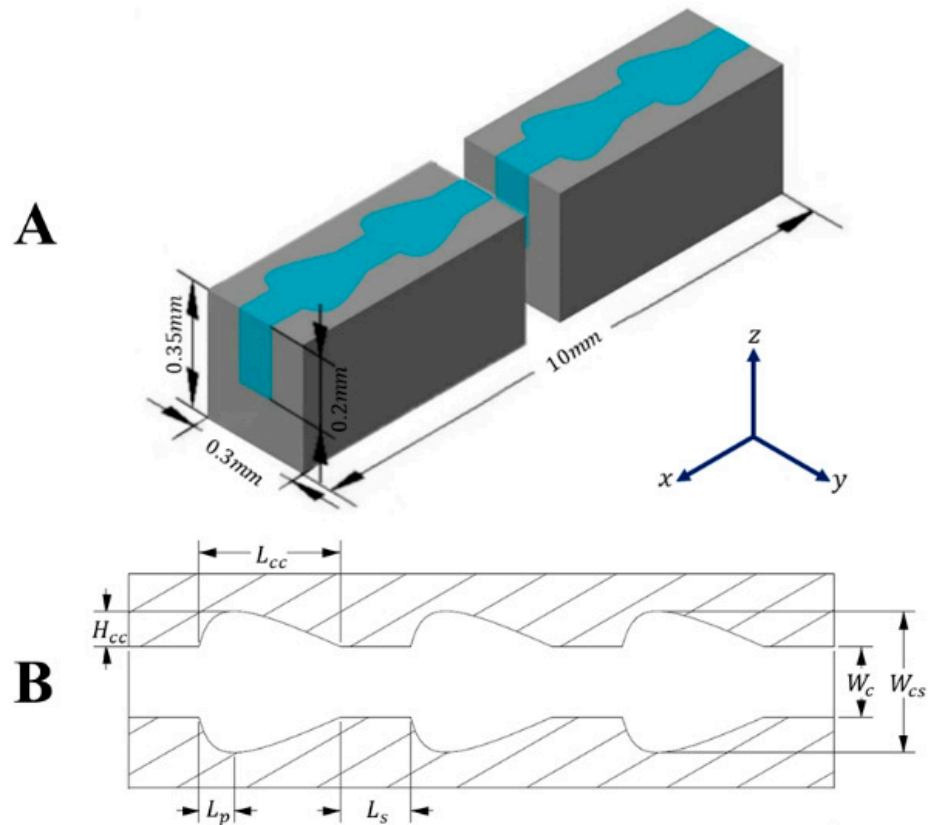- Negligible gravity and radiation heat transfer.

Figure 1. The MCHS with conical-shaped reentrant cavities (**A**) computational domain of the microchannel and (**B**) the geometrical parameters of the new microchannel.

2.2. Governing Equations

As stated in the assumptions for the numerical model, the continuity, momentum, and energy governing equations in the microchannel is given in tensor form as written below.

Continuity equation:

$$\frac{\partial}{\partial x_i}\left(\rho_f u_i\right) = 0 \tag{1}$$

Momentum equation:

$$\frac{\partial}{\partial x_i}\left(\rho_f u_i u_j\right) = \frac{\partial p}{\partial x_j} + \frac{\partial}{\partial x_i}\left[\mu_f\left(\frac{\partial u_j}{\partial x_i} + \frac{\partial u_i}{\partial x_j}\right)\right] \tag{2}$$

Energy equation:

1. For liquid:

$$\frac{\partial}{\partial x_i}\left(\rho_f u_i c_{pf} T_f\right) = \frac{\partial}{\partial x_i}\left(\lambda_f \frac{\partial T_f}{\partial x_i}\right) + \mu_f\left[2\left(\frac{\partial u_i}{\partial x_i}\right)^2 + \left(\frac{\partial u_j}{\partial x_i} + \frac{\partial u_i}{\partial x_j}\right)^2\right] \tag{3}$$

2. For silicon substrate:

$$\frac{\partial}{\partial x_i}\left(\lambda_s \frac{\partial T}{\partial x_i}\right) = 0 \tag{4}$$

2.3. Boundary Conditions

The hydrodynamic boundary conditions are:

$u = v = w = 0$ at the channel wall surface (no-slip and no-penetration);

$u_f = u_{in}$ at the inlet, $x = 0$;

$P_f = P_{out} = 1 atm$ at the outlet, $x = L$.

The thermal boundary conditions are:

1. For liquid

   $T_f = T_{in} = 293K$ at $x = 0$,

   $-\lambda_f \frac{\partial T_f}{\partial x} = 0$ at $x = L$,

2. For silicon substrate by considering the solid region is without axial heat transfer.

   $-\lambda_s \frac{\partial T_s}{\partial x} = 0$ at $x = 0$ and $x = L$,

   $\frac{\partial T_s}{\partial y} = 0$ at $y = 0$ and $y = W$

   $-\lambda_s \frac{\partial T_s}{\partial z} = q$ at $z = 0$,

   $-\lambda_s \frac{\partial T_s}{\partial z} = 0$ at $z = H$,

The Fourier's Law defining the conjugate heat transfer between fluid and solid:

$$-\lambda_f \left(\frac{\partial T_f}{\partial c} \right) = -\lambda_s \left(\frac{\partial T_s}{\partial c} \right) \tag{5}$$

where c is the local coordinate normal to the wall.

The fluid flow properties at the fluid-solid interface were used in calculating the wall shear stress which was acquired by using the velocity gradient at the wall of the MCHS for laminar flow:

$$\tau_f = \mu \left(\frac{\partial u}{\partial c} \right) \tag{5a}$$

2.4. Mesh Precision Test

To diminish the computational time of the numerical simulation, the computational grid of the conventional MCHS was examined at different concentrations while still maintaining the precision of the results. For example, for the microchannel with $\beta = 0.5$, $\delta = 0.75$, and $\gamma = 2.0$ when 1 ms^{-1}, the deviation of Nusselt number for the test done with 0.168, 0.337, and 0.647 million cells from that using 1.110 million cells are 9.76%, 5.92%, and 0.93%, respectively. Therefore, the 0.647 million cells are used for the microchannel with $\beta = 0.5$, $\delta = 0.75$ and, $\gamma = 2.0$. Figure 2 shows the mesh structure used in this numerical simulation. The local refined meshing method is used to fine tune the mesh.
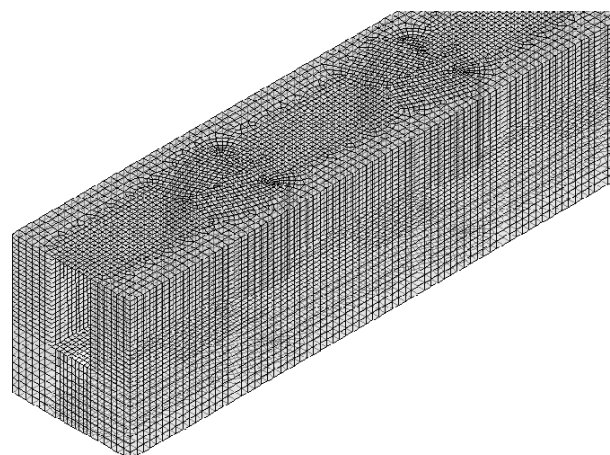

Figure 2. Mesh configuration of the solution domain.

2.5. Numerical Implementation

The governing equations were solved by using ANSYS 17.2 software, Finite Volume Method (FVM) was used with the corresponding boundary conditions. The SIMPLE algorithm was chosen for the flow field analysis while to approximate the convective term, the second-order upwind differencing scheme was adopted. The term of diffusion in the energy and momentum equations is approximated by second-order central difference. Converged results obtained for a residual target of less than 10^{-7} for all variables, but for energy, the equation is 2×10^{-8}.

In the present work, the parameter of interest includes the friction factor, Reynolds number, Nusselt number, and the performance evaluation criterion. The average friction factor is defined as

$$f = \frac{2D_h \Delta p}{\rho L u_m^2} \tag{6}$$

where D_h is the hydraulic diameter calculated from $D_h = 2 W_c H_c / (W_c + H_c)$, W_c and H_c are the width and height of the constant cross-section region of the microchannel, respectively. Δp represents the pressure drop along the total length of the microchannel, L. ρ is the working fluid density and u_m is the mean flow velocity.

The Reynolds number equation is

$$Re = \frac{\rho u_m D_h}{\mu} \tag{7}$$

where μ is the fluid viscosity.

For the fluid flowing through the MCHS, the overall coefficient of heat transfer and the overall Nusselt number were computed as listed below

$$h = \frac{q W_c L}{A \Delta T} \tag{8}$$

$$Nu = \frac{h D_h}{\lambda_f} \tag{9}$$

where q represent the expected heat flux at the bottom surface of the microchannel that was kept constant at 10^6 W/m^2, A ($A = (W_c + 2H_c)L$) is the area of contact between the silicon substrate with the working fluid, ΔT is the temperature difference between the heated bottom of the microchannel and the working fluid which is obtained from $\Delta T = T_{ave} - 0.5(T_{in} + T_{out})$, where T_{ave} is the average temperature at the bottom surface of the microchannel, T_{in} and T_{out} are the inlet and outlet fluid temperature, respectively.

As suggested by Gu et al. [20], the performance evaluation criterion is given by

$$\eta = \frac{\left(Nu_{cs} / f_{cs}^{1/3} \right)}{\left(Nu_{cr} / f_{cr}^{1/3} \right)} \tag{10}$$

3. Results and Discussion

3.1. Numerical Validation

The straight microchannel numerical simulation was validated by comparing the values procured with Steinke & Kandlikar [21] under similar boundary conditions. The frictional pressure drop formulation in the developing region for a rectangular duct is described by Steinke & Kandlikar as follows:

$$\Delta p = \frac{f Re \mu u_m L}{2D_h^2} + K \frac{\rho u_m^2}{2} \tag{11}$$

$$f Re = 96 \left[1 - (1.3553 \cdot AR) + \left(1.9467 \cdot AR^2 \right) - \left(1.7012 \cdot AR^3 \right) + \left(0.9564 \cdot AR^4 \right) - \left(0.2537 \cdot AR^5 \right) \right] \tag{12}$$

$$K = \left(0.6797 + 1.2197AR + 3.3089AR^2 - 9.5921AR^3 + 8.9089AR^4 - 2.9959AR^5\right) \quad (13)$$

where AR is the aspect ratio obtained from $AR = a/b$, a and b are the short and long side, respectively. As illustrated in Figure 3, the pressure drops numerical value is 3.6% less than the results obtained from the above formulations. From this validation, the numerical simulation of all the present microchannels with conical-shaped reentrant cavities are also validated since the same method is adopted.
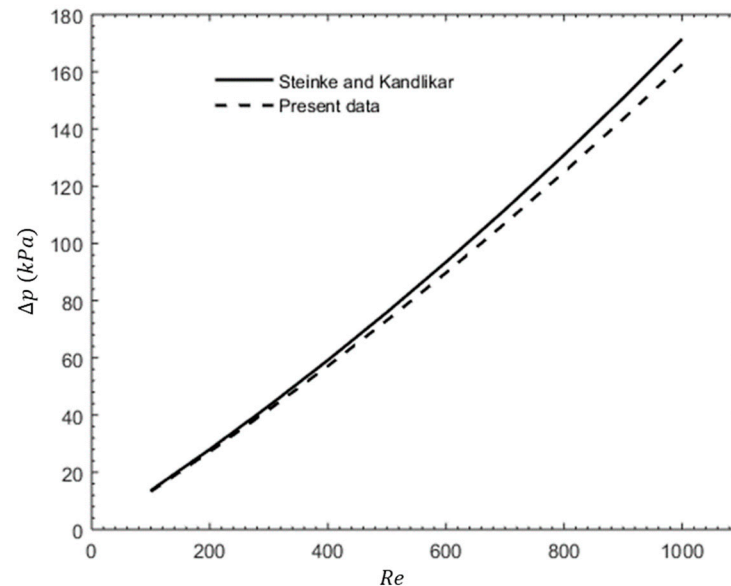

Figure 3. Relationship between Δp and Re for validation of numerical simulation and Steinke Kandlikar formulation results.

3.2. Flow Field Analysis of Conical-Shaped Microchannel Heat Sink

The performance of heat transfer in the current conical-shaped microchannels with the traditional straight microchannel was compared through the analysis of the flow field. According to the study, the regular fluid flow and thickening of the thermal boundary layers lead the heat transfer performance in the traditional straight microchannel to decline across the direction of the fluid flow. A secondary flow, which will improve the working fluid's mixing and hence improve heat transfer performance, may be created while the working fluid travels along a curved path, according to studies [22]. Figure 4A,B shows the velocity vectors, pressure contour, and temperature contour for the conventional MCHS and present CMCHS with $\beta = 0.5$, $\gamma = 1.8$ and $\delta = 0.75$, respectively. The preview plane is located at half of the depth of the working fluid, x is from 7.1 mm to 7.4 mm, and the inlet fluid velocity is 7 m/s. The fluid flow in Figure 4 shows that the flow in conventional MCHS becomes regular throughout the flow direction while the flow in CMCHS is redirected from the mainstream into the cavity area which creates a vortex at the conical-shaped reentrant cavity. The pressure drops in conventional MCHS and shows a linear pattern, while the pressure drop in CMCHS shows a non-linear pattern with a lower pressure at the reentrant region just before the start of the next constant cross-sectional area. The immediate expansion from the previous constant cross-section region leads to a higher pressure as seen by red spots just around the expansion area, which results in lower velocity as indicated by velocity vectors. The temperature profile shows that the conventional MCHS has a 6.3 K higher maximum temperature of compared to the maximum temperature of the CMCHS. The thermal boundary layer in the conventional MCHS is thicker compared to the constant cross-section area of the present CMCHS which causes the heat transfer performance in the conventional MCHS to deplete across the flow direction. In the CMCHS, the temperature at the conical-shaped reentrant cavity is a bit higher compared to the constant cross-section area, especially at the entry point of the cavity.
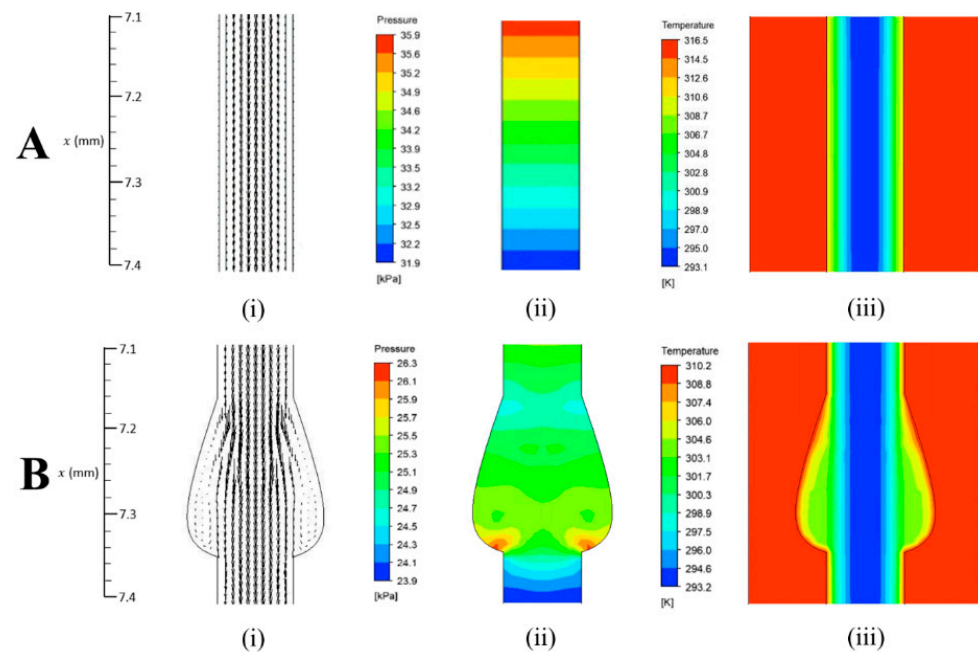
Figure 4. (**i**) velocity vectors, (**ii**) pressure contour and (**iii**) temperature contour for (**A**) conventional MCHS, and (**B**) CMCHS with β = 0.5, γ = 1.8 and δ = 0.75.

Two inferences about the heat transfer enhancement mechanism of the CMCHS may be taken from the analysis above. First off, circulation motions caused by the vortices in the conical-shaped reentrant cavity significantly boost convective fluid mixing. The shear layer that separates the mainstream flow from the flow that recirculates in the conical-shaped reentrant cavity is disrupted by the side-by-side fluid mixing, which passively improves heat transmission. Second, the thermal boundary layer is intermittently disrupted by the discharged and redeveloped fluid flow across the constant cross-section area brought on by the cavity region's expansion. The temperature gradient is widened as a result of this event, increasing the rate of heat transfer.

3.3. Influence of Cavity Number (β)

The thermal and flow performance effects were studied at various values of β at a different u with heat flux of q = 10^6 W/m^2. The remaining parameter is fixed at γ = 2 and δ = 0.75. The β value represent the ratio of the total length of the microchannel respective to the number of cavities introduced ranging from 0.5 to 10 which can be expressed as follows

$$\beta = \frac{L}{n} \tag{14}$$

where n is the number of cavities. The cavity number that corresponds to the value of β is as listed in Table 1.

Table 1. No. of cavities and the corresponding value of β.

Number of Cavities	1	2	4	5
β	10	5	2.5	2
Number of Cavities	8	10	16	20
β	1.25	1	0.625	0.5

Figure 5 shows that the current microchannels with conical-shaped reentrant cavities improves the performance of heat transfer as being compared to the conventional straight microchannel. Figure 5 also shows that Nu_{cs}/Nu_{cr} decreases as β increases. When the inlet velocity was set at 1 m/s, the Nu_{cs}/Nu_{cr} decreases gradually for β value from 0.5 to 1,

and then it became almost consistent until $\beta = 10$. When the inlet velocities are at 4 m/s and 7 m/s, the value of Nu_{cs}/Nu_{cr} decreases drastically when β value is from 0.5 to 1 and then decreases gradually until $\beta = 10$. The thermal enhancement is significantly higher at higher velocity and the value converges with the thermal enhancement at lower velocity as β reaches 10. When $\beta = 0.5$ for u = 7 m/s, the Nusselt number reached 1.47 times higher compared to the straight microchannel.
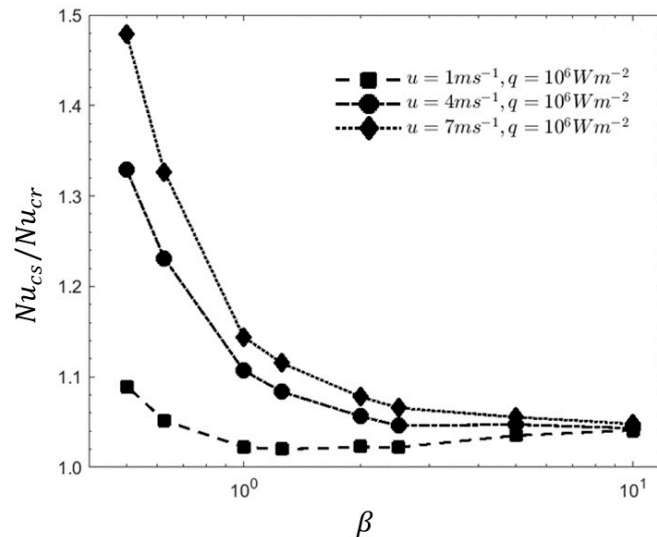
Figure 5. Nu_{cs}/Nu_{cr} against β.

The increase in friction factor will simultaneously increase the pressure drop. To evaluate, the performance evaluation criterion (η) was adopted as the heat transfer enhancement standard evaluation method. In Figure 6, the trend shows that when at a higher value of β, the cavities are arranged further from each other by a significant distance, causing the thermal boundary layer to grow back to a fully developed condition after passing each of the cavity. This condition remains until the flow reaches the next cavity. Therefore, the increment of the thermal performance is not too much. At lower β value, the disturbance and development of the boundary layer becomes more frequent, causing in a higher η. As the number of cavities in the MCHS increases, it produces further chaotic advection in the MCHS which contributes towards a higher heat transfer performance. The highest performance can be observed at $\beta = 0.5$ when the velocity is at 7 m/s, where the value of η increases up to 1.49.
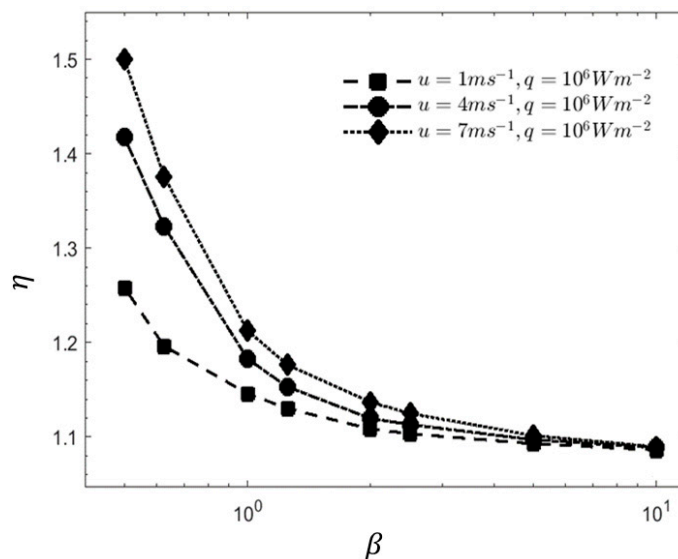

Figure 6. η against β.

3.4. Influence of Cavity Width (γ)

The thermal and flow performance effects was studied at various values of γ and at different u, with $\beta = 0.5$ and heat flux of q = 10^6 W/m^2. The remaining parameter was fixed at $\delta = 0.75$. It is known that γ is the ratio between the largest width of the conical cavity's sidewalls to the constant cross-section region of the MCHS and is written as

$$\gamma = \frac{W_{cs}}{W_c} \tag{15}$$

Since the size of each of the cavity is set to be constant at 0.2 mm, the increment of γ value directly represents the enlargement of the cavity size. Figure 7 shows that when u = 1 m/s, the Nu_{cs}/Nu_{cr} value decreases at γ ranging from 1.3 to 1.4, then the value increases steadily from 1.4 until 1.8, then remains almost constant until it reaches 2.0. Overall, the Nu_{cs}/Nu_{cr} values at u = 1 m/s show minimal changes and remains within 1.0 and 1.1. At u = 4 m/s, the Nu_{cs}/Nu_{cr} values increase from $\gamma = 1.3$ to 1.4, but the ratio decreases for u = 7 m/s at the same value of γ. From γ value of 1.5 to 2.0, the Nusselt number ratio fluctuates. The pattern is the same for both u values of 4 m/s and 7 m/s, but with different amplitude. The Nu_{cs}/Nu_{cr} value when u = 4 m/s is higher than at 7 m/s for γ value from 1.6 to 1.9. This indicates the complement of the transverse vortices with the conical-shaped reentrant cavity. Due to regular variation of the friction factor with γ value, the proclivity of η with γ as shown in Figure 8 shows the same form as the Nu_{cs}/Nu_{cr}, but with different amplitude. The result presented in Figure 7 is in good agreement with the results presented by Xia et al. [9].
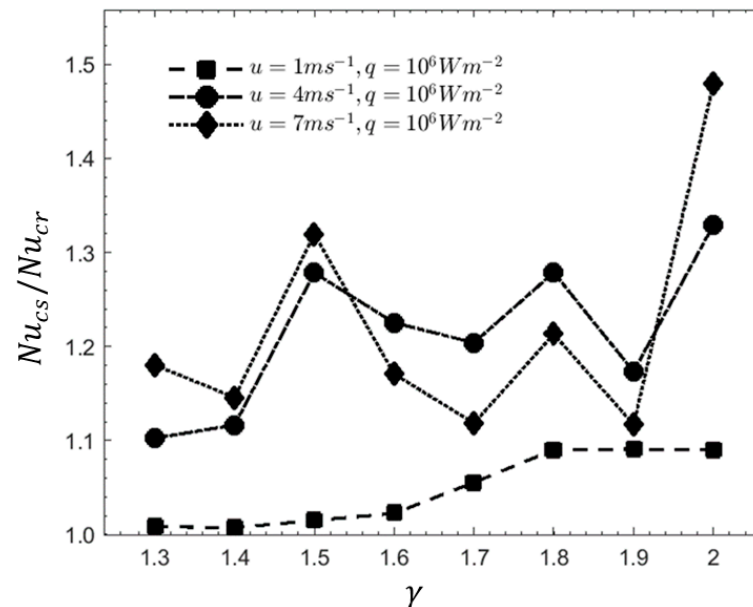

Figure 7. Nu_{cs}/Nu_{cr} against γ.

The velocity vectors, pressure contour, and temperature contour shown in Figure 9A,B, with cavity width ratio of $\gamma = 1.4$ and $\gamma = 2.0$, respectively, shows a clear comparison at u = 7 m/s with the flow direction from the upper part. As can be seen, in Figure 9A, there is only a small flow separation due to limited space in the reentrant cavity region as compared to in Figure 9B. The velocity vectors show a greater flow eddies recirculation inside the larger cavity width, allowing the fluid to transfer out more heat from the sidewalls. This recirculation creates vortices inside the cavity region which decreases the thickness of the thermal boundary layer, thus reducing the thermal resistance. Figure 9 shows that when γ value increases, the heat transfer surface area also increases. The vortices created helps to direct the cold fluid from the mainstream flow to move towards the wall of the cavity which allows the fluid to absorb more heat from the sidewalls. The flow separation is enhanced

as a result from the higher pressure drop across the reentrant cavity area which forces the fluid to be recirculated before going back into the mainstream. This greater pressure drop results in better mixing of fluid, thus augmenting the heat transfer performance.
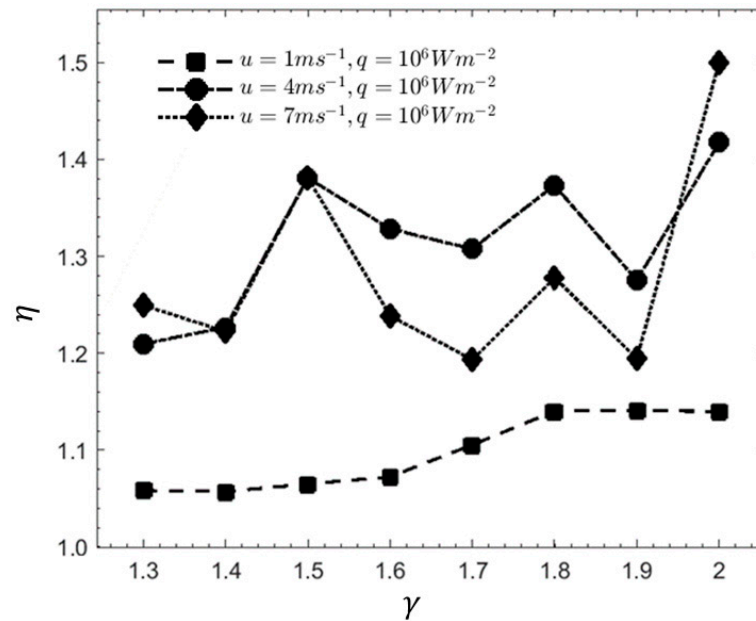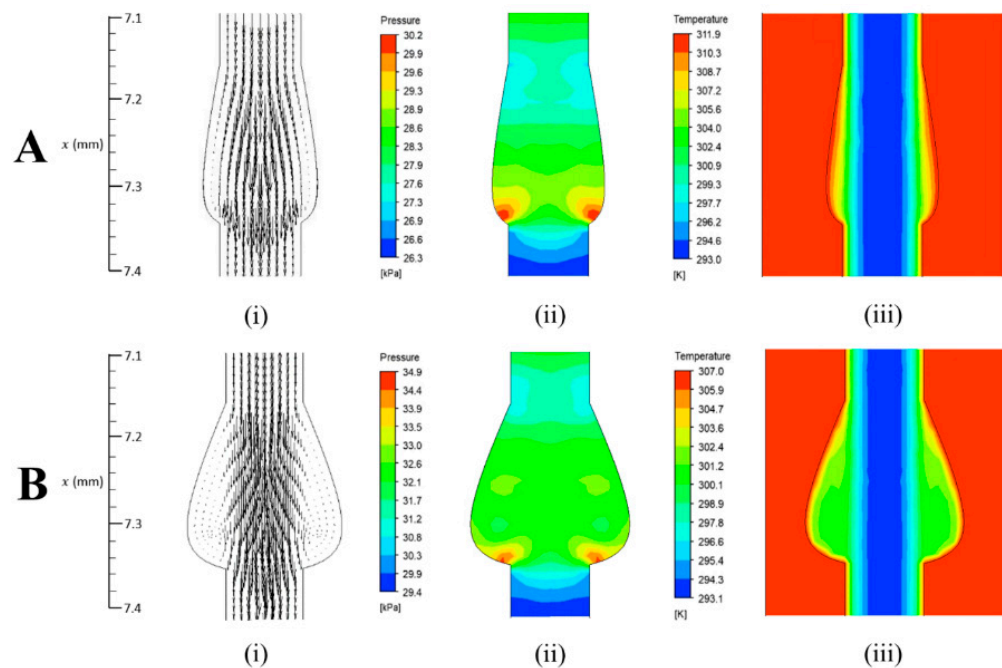

Figure 8. η against γ.

Figure 9. (**i**) velocity vectors, (**ii**) pressure contour and (**iii**) temperature contour for the microchannel with parameters at (**A**), $\beta = 0.5$, $\gamma = 1.4$, and $\delta = 0.75$, and at (**B**), $\beta = 0.5$, $\gamma = 2.0$, and $\delta = 0.75$.

3.5. Influence of Peak Distance from the Entrance of Each Cavity (δ)

The thermal and flow performance effects was studied at various values of δ and at different u with $\beta = 0.5$ and $\gamma = 2.0$. δ is the ratio of the peak distance from the entrance of each cavity with the total length of the conic cavity and is written as

$$\delta = \frac{L_p}{L_{cc}} \tag{16}$$

The growth of δ directly represents the position of the peak point form the entrance of the cavity and the value of δ ranging from 0.15 to 0.85. The result as presented in Figure 10 shows that for all values of u, as the value of δ increases from $\delta = 0.15$ to $\delta = 0.35$, the value of Nu_{cs}/Nu_{cr} decreases. For u = 1 m/s, the minimum value of Nu_{cs}/Nu_{cr} was reached at $\delta = 0.35$, and then the value increased gradually until $\delta = 0.75$. There was only a slight increase of the Nu_{cs}/Nu_{cr} value from $\delta = 0.75$ to $\delta = 0.85$. At u = 4 m/s and 7 m/s, the Nu_{cs}/Nu_{cr} value continued to decrease after $\delta = 0.35$ until it reached the minimum value at $\delta = 0.45$. The Nu_{cs}/Nu_{cr} then increased to its peak value at $\delta = 0.75$, where it clearly showed that the design had reached its optimal cavity entrance angle before drastically dropping at $\delta = 0.85$. The friction factor ratio, f_{cs}/f_{cr}, had a regular variation with δ, causing a similar pattern of η against δ and the Nu_{cs}/Nu_{cr} against δ with different amplitude, as shown in Figure 11.
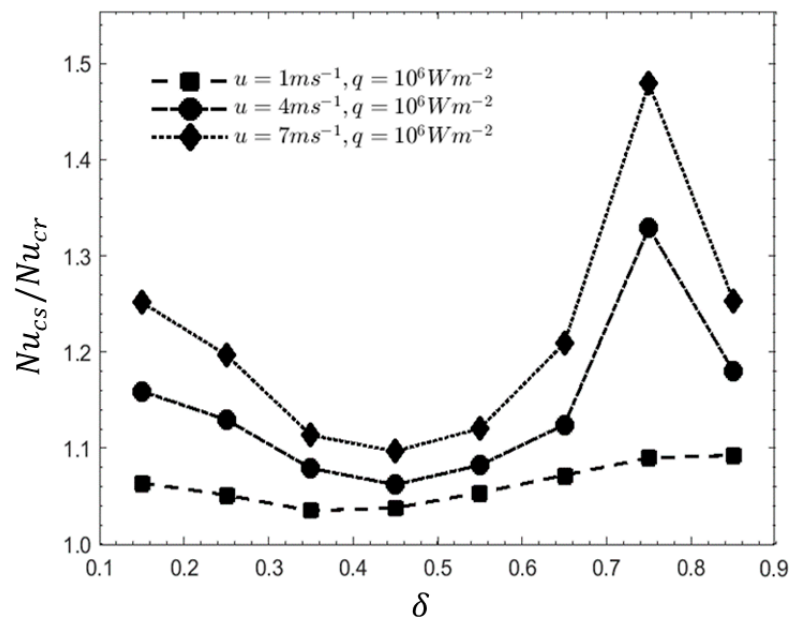
Figure 10. Nu_{cs}/Nu_{cr} against δ.

Figure 11. η against δ.
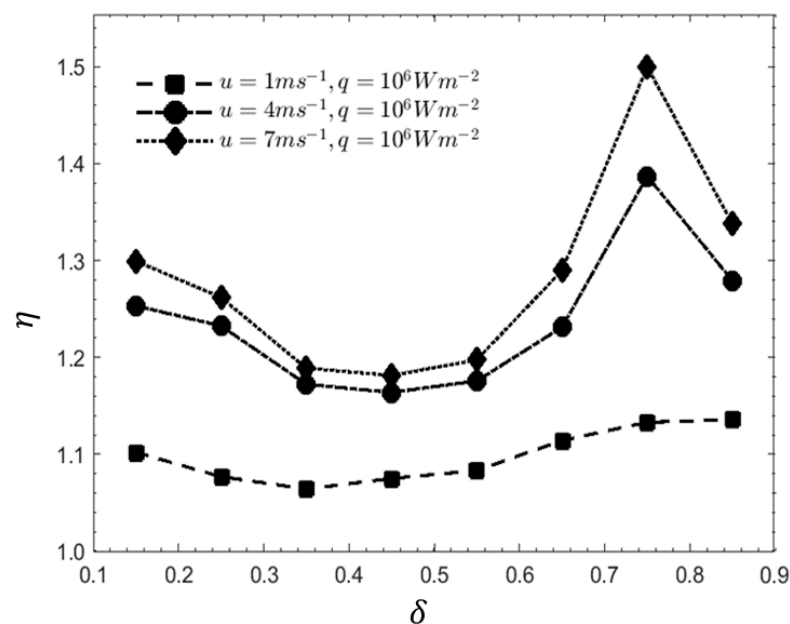
The velocity vectors, pressure contour and temperature contour for δ = 0.15 and 0.85, respectively, as β = 0.5, γ = 2.0 and u = 7 m/s were presented in Figure 12A,B. The fluid flow in Figure 12A shows that as the flow from the mainstream passes through the conical-shaped reentrant cavity, the flow separates and moves towards the sidewalls which creates a vortex flow. The vortex formed was caused by the reverse pressure difference across the reentrant cavity. However, the included angle of the sidewall at the inlet of the reentrant cavity to the direction of the mainstream flow is at its maximum value, creating a laminar stagnation zone. At the inlet of the reentrant cavity, the laminar stagnation zone has badly impacted the heat transfer rate. The laminar stagnation zone kept on getting bigger as the peak position moved closer to the center of the cavity, causing less heat to be transferred out. As shown in Figure 9B, for δ = 0.75, where all of the other parameters were set to be similar, the laminar stagnation zone was at its minimum as the included angle between the inlet reentrant cavity sidewall and the mainstream flow direction wass at the optimum position which subsequently brought the performance of the heat transfer to the maximum point.
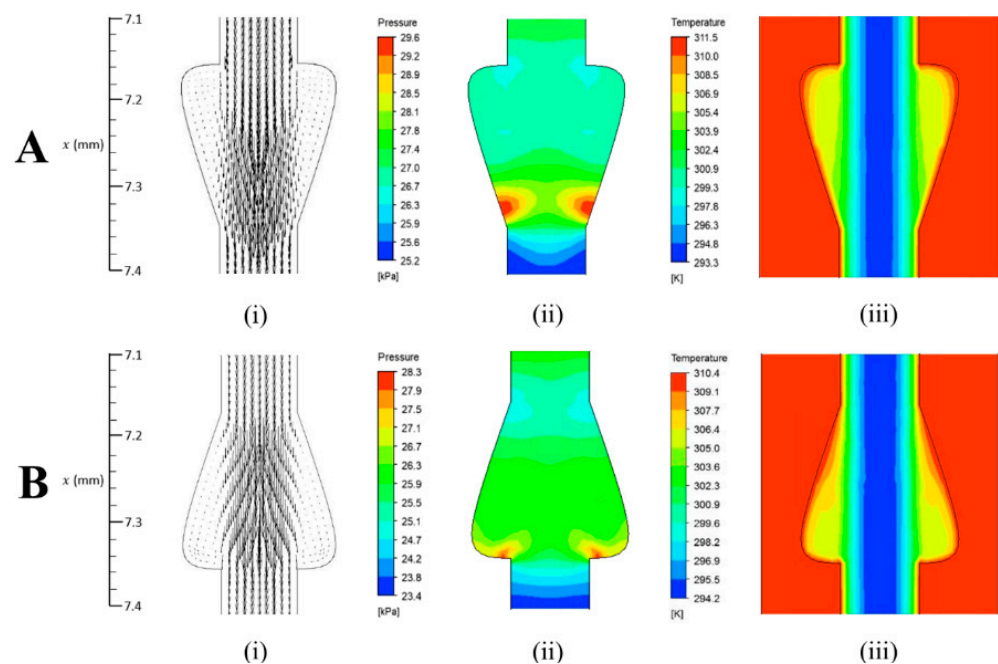

Figure 12. (**i**) velocity vectors, (**ii**) pressure contour and (**iii**) temperature contour for the microchannel with parameters at (**A**), β = 0.5, γ = 2.0 and δ = 0.15 and at (**B**), β = 0.5, γ = 2.0 and δ = 0.85.

4. Conclusions

The result of current work can be summarized as follows:

The heat transfer and fluid flow in the conical-shaped microchannel can be mainly attribute to the redeveloping boundary layer, the increase around heat transfer surface, and the slipping over the reentrant cavities provided by the conical-shaped reentrant cavities. The formed vortex inside the reentrant cavities les to chaotic advection and convective fluid mixing. It also interrupted and periodically redeveloped the thermal boundary layer along the constant cross-section surface.

A higher fluid inlet velocity can increase the magnitude of the vortex formed while simultaneously reducing the thermal boundary layer across the constant cross-section region. As the inlet velocity increases, it requires a higher penalty of pressure drop to further increase the heat transfer performance.

The results shows that the conical-shaped reentrant cavity with the parameters β = 0.5, γ = 2.0, δ = 0.75, and u = 7 m/s provides a Nusselt number ratio enhancement of 1.47, which is the optimum thermal design for the CMCHS. Overall, there is a notable enhancement of heat transfer in the new microchannel with conical-shaped reentrant cavity. This stipulates the effectiveness of using CMCHS when the current boundary conditions were applied.

Nomenclature

A	Contact surface area between water and silicon	m^2
AR	Aspect ratio	-
c	local coordinate normal to the wall	-
c_p	Specific heat capacity	J/kg·K
D_h	Hydraulic diameter	m
f	Friction factor	-
H	Height of the microchannel	m
h	Heat transfer coefficient	W/m²·K
K	Hagenbach factor	-
L	Length of the microchannel	m
n	Number of cavities	-
Nu	Nusselt number	-
p	Pressure	kPa
q	Projected heat flux on the bottom of the microchannel	W/m^2
Re	Reynolds number	-
T	Temperature	K
u	Velocity	m/s
W	Total width of microchannel plus lateral wall	m
x, y, z	Dimensionless Cartesian coordinate	-
Greek letters		
β	Ratio of the total length of the channel respective to the number of cavities introduced	-
γ	Ratio of the largest width of the conical cavities side wall with the constant cross-section	-
δ	Ratio of the peak distance from the entrance of each cavity with the total length of the conic cavity	-
η	Performance evaluation criterion	-
λ	Thermal conductivity	W/m·K
μ	Dynamic viscosity	Pa·s
ρ	Density	kg/m^3
τ	Wall shear stress	N

Subscript
ave   Average
c   Channel
cc   Conic cavity
cr   Conventional rectangular
cs   Conic shape
f   Fluid
i, j, k x, y, z direction of Cartesian coordinate
in   Inlet
m   Mean
out   Outlet
p   Peak
s   Silicon
sc   Space between cavity

References

1. Tuckerman, D.B.; Pease, R.F.W. High-performance heat sinking for VLSI. *IEEE Electron Device Lett.* **1981**, *2*, 126–129. [CrossRef]
2. Mohamad Noh, N.H.; Che Sidik, N.A. Numerical Simulation of Nanofluids for Improved Cooling Efficiency in Microchannel Heat Sink. *Appl. Mech. Mater.* **2014**, *695*, 403–407. [CrossRef]
3. Peng, X.F.; Peterson, G.P. Convective heat transfer and flow friction for water flow in microchannel structures. *Int. J. Heat Mass Transf.* **1996**, *39*, 2599–2608. [CrossRef]
4. Adams, T.M.; Abdel-Khalik, S.I.; Jeter, S.M.; Qureshi, Z.H. An experimental investigation of single-phase forced convection in microchannels. *Int. J. Heat Mass Transf.* **1998**, *41*, 851–857. [CrossRef]
5. Tao, W.Q.; He, Y.L.; Wang, Q.W.; Qu, Z.G.; Song, F.Q. A unified analysis on enhancing single phase convective heat transfer with field synergy principle. *Int. J. Heat Mass Transf.* **2002**, *45*, 4871–4879. [CrossRef]
6. Steinke, M.E.; Kandlikar, S.G. Single-phase heat transfer enhancement techniques in microchannel and minichannel flows. In Proceedings of the Second International Conference on Microchannels and Minichannels, Rochester, NY, USA, 17–19 June 2004; pp. 141–148.
7. Gunnasegaran, P.; Mohammed, H.A.; Shuaib, N.H.; Saidur, R. The effect of geometrical parameters on heat transfer characteristics of microchannels heat sink with different shapes. *Int. Commun. Heat Mass Transf.* **2010**, *37*, 1078–1086. [CrossRef]
8. Alfaryjat, A.A.; Mohammed, H.A.; Adam, N.M.; Ariffin, M.K.A.; Najafabadi, M.I. Influence of geometrical parameters of hexagonal, circular, and rhombus microchannel heat sinks on the thermohydraulic characteristics. *Int. Commun. Heat Mass Transf.* **2014**, *52*, 121–131. [CrossRef]
9. Xia, G.; Chai, L.; Zhou, M.; Wang, H. Effects of structural parameters on fluid flow and heat transfer in a microchannel with aligned fan-shaped reentrant cavities. *Int. J. Therm. Sci.* **2011**, *50*, 411–419. [CrossRef]
10. Chai, L.; Xia, G.; Zhou, M.; Li, J. Numerical simulation of fluid flow and heat transfer in a microchannel heat sink with offset fan-shaped reentrant cavities in sidewall. *Int. Commun. Heat Mass Transf.* **2011**, *38*, 577–584. [CrossRef]
11. Xia, G.; Chai, L.; Wang, H.; Zhou, M.; Cui, Z. Optimum thermal design of microchannel heat sink with triangular reentrant cavities. *Appl. Therm. Eng.* **2011**, *31*, 1208–1219. [CrossRef]
12. Chai, L.; Xia, G.; Wang, L.; Zhou, M.; Cui, Z. Heat transfer enhancement in microchannel heat sinks with periodic expansion-constriction cross-sections. *Int. J. Heat Mass Transf.* **2013**, *62*, 741–751. [CrossRef]
13. Abouali, O.; Baghernezhad, N. Numerical Investigation of Heat Transfer Enhancement in a Microchannel With Grooved Surfaces. *J. Heat Transf.* **2010**, *132*, 041005. [CrossRef]
14. Kuppusamy, N.R.; Mohammed, H.A.; Lim, C.W. Numerical investigation of trapezoidal grooved microchannel heat sink using nanofluids. *Thermochim. Acta* **2013**, *573*, 39–56. [CrossRef]
15. Ahmed, H.E.; Ahmed, M.I. Optimum thermal design of triangular, trapezoidal and rectangular grooved microchannel heat sinks. *Int. Commun. Heat Mass Transf.* **2015**, *66*, 47–57. [CrossRef]
16. Li, Y.F.; Xia, G.D.; Ma, D.D.; Jia, Y.T.; Wang, J. Characteristics of laminar flow and heat transfer in microchannel heat sink with triangular cavities and rectangular ribs. *Int. J. Heat Mass Transf.* **2016**, *98*, 17–28. [CrossRef]
17. Ghani, I.A.; Kamaruzaman, N.; Sidik, N.A.C. Heat transfer augmentation in a microchannel heat sink with sinusoidal cavities and rectangular ribs. *Int. J. Heat Mass Transf.* **2017**, *108*, 1969–1981. [CrossRef]
18. Lin, L.; Zhao, J.; Lu, G.; Wang, X.D.; Yan, W.M. Heat transfer enhancement in microchannel heat sink by wavy channel with changing wavelength/amplitude. *Int. J. Therm. Sci.* **2017**, *118*, 423–434. [CrossRef]
19. Alfellag, M.A.; Ahmed, H.E.; Fadhil, O.T.; Kherbeet, A.S. Optimal hydrothermal design of microchannel heat sink using trapezoidal cavities and solid/slotted oval pins. *Appl. Therm. Eng.* **2019**, *158*, 113765. [CrossRef]
20. Gu, W.Z.; Shen, J.Y.; Ma, C.F. *Heat Transfer Enhancement*; Science Press: Beijing, China, 1990.
21. Steinke, M.E.; Kandlikar, S.G. Single-phase liquid friction factors in microchannels. *Int. J. Therm. Sci.* **2006**, *45*, 1073–1083. [CrossRef]
22. Sui, Y.; Teo, C.J.; Lee, P.S.; Chew, Y.T.; Shu, C. Fluid flow and heat transfer in wavy microchannels. *Int. J. Heat Mass Transf.* **2010**, *53*, 2760–2772. [CrossRef]